Frequency Generalization via Darboux Bivector and Electrical Curves in Multi-Phase Power Systems

Francisco G. Montoya, Jorge Ventura, Francisco Arrabal-Campos, Alfredo Alcayde and Ahmad H. Eid

***Abstract*—This paper investigates the concept of frequency in arbitrary multi-phase systems based on geometrical principles. The proposed approach relies on state-of-the-art mathematical techniques such as differential geometry and geometric algebra in n dimensions. By analyzing the generalized Frénet-Serret frame, we derive how the Darboux bivector can accurately express the rotation of this frame as a rigid body in space. It is shown how the concept of frequency in power grids can be intimately linked to spatial rotations. New insights are presented based on the comparison with other recently published works. It is also concluded that the application to single-phase systems cannot always be accommodated by spatial curves. Several examples are used to illustrate the findings of this paper.**

***Index Terms*—Geometric Electricity, Geometric Algebra, Differential Geometry, Frequency, Multi-phase Systems, Electric Curves.**

I. Introduction

THE study of power systems is crucial for the proper management and operation of the power grid. In this sense, voltage or frequency control plays a fundamental role in its stability [1]. The use of appropriate mathematical tools is very important for this task. However, engineers end up overwhelmed by the extensive and heterogeneous number of them to tackle the analysis process with certain guarantees. The not-so-exhaustive list includes complex numbers and phasors [2], quaternions [3], matrices [4], tensors [5] or differential forms [6]. In addition, it is common to find a combination of them, which unnecessarily complicates the analysis or causes it to be difficult to understand. In this sense, Geometric Algebra (GA) provides a unifying vision as a universal framework for engineering and physics [7], [8]. It not only offers a unique framework for the study of electrical systems [9]–[12] but also enables the study of other fields (such as differential geometry, DG) from a multidimensional and comprehensive perspective [13]. However, its application is rather limited in the engineering field, so more work is needed to highlight the benefits of the GA framework.

As a result of this unifying view, it is possible to address outstanding challenges with greater consistency. For example, there is an abundance of literature studying transient events in dynamic conditions, where the complexity of accurate estimations of the grid frequency is highlighted [14]–[16]. Recently, this issue has been emphasized in two papers [17], [18] where the role of differential geometry and geometric algebra in the study of electrical systems and circuits is underlined. In [17] an interesting geometrical interpretation of the frequency of electrical circuits is established through the definition of a multivector that has a symmetrical and an antisymmetrical part. This multivector is obtained from the study of spatial curves representing the magnetic flux of the different phases of a circuit. Although this work envisions the possibility of working with arbitrary dimensions, this aspect is not explored in depth. Interestingly, in [18] the promising GA line is abandoned in favour of an approach focused exclusively on DG. It proposes the use of the Frénet-Serret frame and intrinsic properties of curves such as the curvature and torsion invariants. The concept of geometrical frequency and its relation to current and voltage derivatives is further elaborated. However, certain aspects need deeper investigations for clarity. For example, the extension to systems of more than three phases (dimensions) is not presented (although it is outlined in [17]). It could be of interest in important applications such as multi-phase electrical machines [19] and power converters [20]. Moreover, the interpretation provided for single-phase systems and DC suffers from some hard-to-fit aspects. From a physical point of view, there is no flux to rely on in a DC or a purely resistive circuit. Therefore, building a spatial curve and finding its intrinsic properties is not completely justified.

In this work, we exploit the application of geometric algebra and differential geometry to electrical engineering and power systems by characterizing the voltage (current) of a multi-phase AC system using spatial curves in n dimensions. We'll refer to them as *electrical curves* (EC). This approach allows the study of important properties in multi-phase power systems from a purely geometric point of view. In particular, the definition of frequency extended to arbitrary n phases is provided. This is a significant breakthrough for multi-phase systems, where none of the individual phases can faithfully characterize the entire system and its properties.

Similar to [12], the use of time derivatives plays a fundamental role in determining the underlying properties of the electrical curves, and hence, of the electrical systems.

A. Contributions

The main contributions and novelties of this paper are based on the following aspects:

- Application of geometric algebra and differential geometry to extend the concept of geometric frequency for arbitrary multi-phase systems.
- Introduction of the Darboux bivector (DB) for electrical curves. It generalizes the plane of rotation of the Frénet-Serret frame for n dimensions and links the angular velocity to the generalized geometric frequency. The derivative of DB also generalizes the concept of RoCoF.
- Introduction of the scaled curvatures.
- Introduction of a time-dependent geometric rotor function $\boldsymbol{R}(t)$ to transform phase coordinates to constant Frénet-Serret frame coordinates.
- Determination of restrictions for the validity of the method in single-phase and DC circuits.
- Unified mathematical formulation for electrical engineering and differential geometry concepts based on the use of geometric algebra that improves understanding at the

educational level through visualization techniques widely used in other engineering disciplines.

B. Outline

The outline of the paper is as follows. Section II presents the basic concepts of geometric algebra and its application to classical differential geometry. The concepts of *bivector* and *geometric rotor* are introduced to model rotations in n-dimensional spaces without the use of matrices. Section III discusses the application of the developed model in Section II to power systems. In this context, the Darboux bivector is introduced to represent the instantaneous plane of rotation of the Frénet-Serret frame. Section IV presents the main analytical derivations for sinusoidal AC systems. Some examples are provided in section V to highlight the benefits and validate the proposed approach. Section VI draws some conclusions and Section VII outlines future work.

II. Differential Geometry in the Geometric Algebra formalism

Differential geometry is the study of the geometry of manifolds. It is widely used today in many disciplines, including architecture, computer vision, computer graphics, engineering, and physics. Historically, techniques based on linear algebra and vector calculus have been commonly deployed to apply in DG. Interestingly enough, large parts of vector calculus are confined to $\mathbb{R}^3$ due to the extensive use of the cross product. However, other formalisms like tensors and differential forms must be used to extend to higher dimensions. In contrast, GA provides an at once simpler and more powerful way to deal with these issues because it enables the development of several new methods for coordinate-free DG on manifolds of any dimension. Is the authors' belief that GA will make differential geometry more accessible to readers who have at least completed a basic course in linear algebra.

A. Geometric Algebra basics

GA is "the new kid on the block" in a sense. Nevertheless, it is merely a powerful mathematical method that has been attracting the attention of researchers in recent years. Its application to general problems in electrical engineering is gaining increasing acceptance. However, its use is still limited, perhaps because of the traditional avoidance of change that any new methodology entails. In this section, a quick overview is given of the most basic foundations that allow its elementary knowledge and the application to the developments of this work. The reader is referred to references [7] and [13] for further details.

The process starts with the definition of a Euclidean orthonormal basis in $\mathbb{R}^n$

$$\boldsymbol{\sigma} = \{\boldsymbol{\sigma}_1, \boldsymbol{\sigma}_2, \ldots, \boldsymbol{\sigma}_n\} \tag{1}$$

with basic properties

$$\begin{aligned} \boldsymbol{\sigma}_i \cdot \boldsymbol{\sigma}_i &= 1 \qquad \text{for } i = 1, \ldots, n \\ \boldsymbol{\sigma}_i \cdot \boldsymbol{\sigma}_j &= 0 \qquad \text{for } i \neq j \end{aligned} \tag{2}$$

Any vector $\boldsymbol{v}$ of this space can be considered as a linear combination of the given orthonormal basis $\boldsymbol{\sigma}$

$$\boldsymbol{v} = \sum_{i=1}^{n} v_i \boldsymbol{\sigma}_i = v_1 \boldsymbol{\sigma}_1 + \ldots + v_n \boldsymbol{\sigma}_n \tag{3}$$

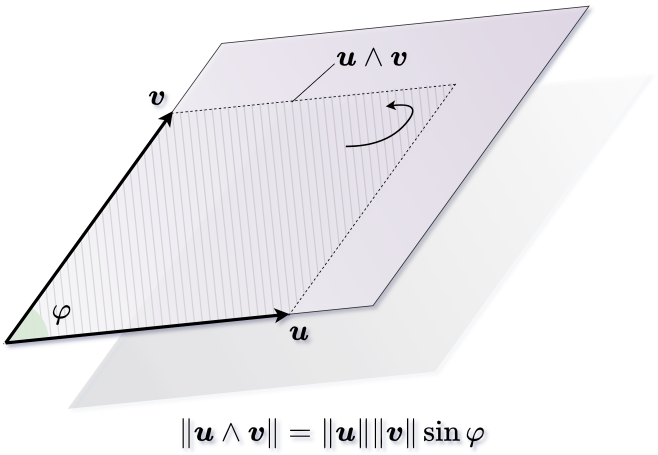

Figure 1. Representation of a simple bivector generated by vector $\boldsymbol{u}$ and $\boldsymbol{v}$. Note that $\boldsymbol{u} \wedge \boldsymbol{v}$ has a direction (the same as the generated plane), sense (indicated by the arrow, from $\boldsymbol{u}$ to $\boldsymbol{v}$) and magnitude (the area of the hatched rectangle).

Note that, so far, we have only used simple and widely known concepts in linear algebra. The relevant parts entail the use of Grassmann's exterior algebra [21] and Clifford's geometric algebra [22]. The former defines an axiomatic bilinear operation for vectors:

$$\boldsymbol{v} \wedge \boldsymbol{v} = 0 \tag{4}$$

i.e., the wedge or exterior product of a vector by itself is null. This property automatically implies that the wedge product is an anticonmutative operation, i.e., given two non-collinear vectors $\boldsymbol{u}$ and $\boldsymbol{v}$, the following is satisfied

$$\boldsymbol{u} \wedge \boldsymbol{v} = -\boldsymbol{v} \wedge \boldsymbol{u} \tag{5}$$

The wedge product of two vectors builds up a new geometric entity: the (simple) bivector $\boldsymbol{u} \wedge \boldsymbol{v}$. It represents a 2-dimensional object (a plane) with direction, sense, and magnitude (see Fig. 1). All bivectors in 2D and 3D are simple, i.e., they are always a product of 2 vectors. This is not the case for higher dimensions [23], where a bivector is the sum of simple bivectors. Moreover, by wedging more vectors together, new high-dimensional objects (k-vectors) can be constructed. For example, in a 4-dimensional space, the wedge product of 4 different non-collinear vectors gives a quadvector, i.e., a hypervolume object.

Finally, the geometric product[1] is defined as an invertible bilinear operation

$$\boldsymbol{u}\boldsymbol{v} = \boldsymbol{u} \cdot \boldsymbol{v} + \boldsymbol{u} \wedge \boldsymbol{v} \tag{6}$$

which is the sum of the inner and the wedge product. Using properties (2) and (4), the geometric product among basis vectors fulfills

[1] Although Clifford made great contributions to geometric algebra, the geometric product has been erroneously attributed to him [24]. However, it was Marcel Riesz who first proposed it formally.

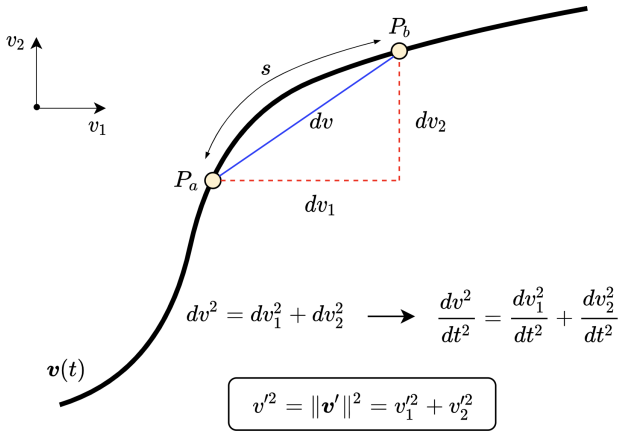

Figure 2. Determination of arclength s in a 2D space curve $\boldsymbol{v}$. For parameters $t = a$ and $t = b$, two points P_a and P_b can be mapped on the curve. The length between these points is s and it can be determined using the derivative $\boldsymbol{v}'$, i.e. when P_b approaches P_a.

$$\begin{aligned} \boldsymbol{\sigma}_i^2 &= \boldsymbol{\sigma}_i\boldsymbol{\sigma}_i = \boldsymbol{\sigma}_i \cdot \boldsymbol{\sigma}_i = 1 \qquad \text{for } i = 1, \ldots, n \\ \boldsymbol{\sigma}_i\boldsymbol{\sigma}_j &= \boldsymbol{\sigma}_{ij} = -\boldsymbol{\sigma}_{ji} = \boldsymbol{\sigma}_i \wedge \boldsymbol{\sigma}_j \qquad \text{for } i \neq j \\ (\boldsymbol{\sigma}_i\boldsymbol{\sigma}_j)^2 &= \boldsymbol{\sigma}_i\boldsymbol{\sigma}_j\boldsymbol{\sigma}_i\boldsymbol{\sigma}_j = -\boldsymbol{\sigma}_i\boldsymbol{\sigma}_i\boldsymbol{\sigma}_j\boldsymbol{\sigma}_j = -1 \end{aligned} \tag{7}$$

In GA, different k-vectors can be added up to form a multivector $\boldsymbol{M}$. The norm of a multivector is:

$$\boldsymbol{M} = \sqrt{\langle \boldsymbol{M}^\dagger \boldsymbol{M} \rangle_0} \tag{8}$$

where $\boldsymbol{M}^\dagger$ is the reverse operation and the operator $\langle\cdot\rangle_0$ refers to the scalar part of a multivector (see [7] for more details). Note that bold capital letters are used for multivectors (including bivectors) and bold small letters for vectors. Scalars are represented by non-bold letters.

B. Differential Geometry for space curves using GA

The classical study of space curves is accomplished by means of DG. For this purpose, one usually defines an n-dimensional curve in parametric form within a given interval. Mathematically, it is denoted as $\boldsymbol{v} : t \in [a, b] \to \mathbb{R}^n$. Note that the vector given in (3), with $v_i = v_i(t)$ being dependent on the parameter t, can be used for the representation of the curve $\boldsymbol{v}$ respect to the fixed orthonormal frame $\boldsymbol{\sigma}$. The length between two arbitrary points of this curve, P_a and P_b (see Fig. 2 for a simple case with $n = 2$), can be computed as

$$s = \int_a^b \|\boldsymbol{v}'(t)\| dt \tag{9}$$

where

$$\boldsymbol{v}'(t) = \frac{d\boldsymbol{v}(t)}{dt} = \sum_{i=1}^{n} v_i'(t)\boldsymbol{\sigma}_i \tag{10}$$

is the first derivative of the curve $\boldsymbol{v}$ respect to parameter t (also known as *speed*) and

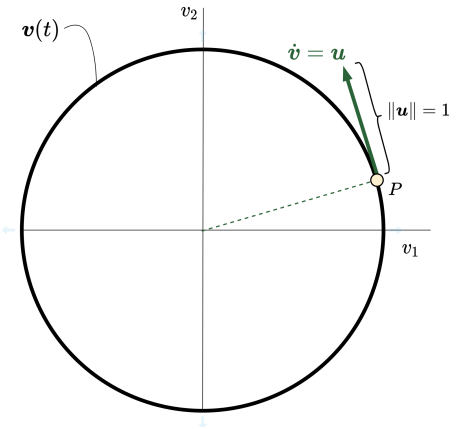

Figure 3. Tangent vector $\boldsymbol{u}$ to curve $\boldsymbol{v}$ at point P. This vector has a unitary length by definition.

$$\|\boldsymbol{v}'\|^2 = v'^2 = \boldsymbol{v}' \cdot \boldsymbol{v}' = \sum_{i=1}^{n} v_i'^2 \tag{11}$$

is the norm of $\boldsymbol{v}'$. From now on, parameter t will be omitted unless otherwise stated.

1) Arc-Length reparametrization and the role of derivatives: A very common practice in DG is to perform a reparametrization of the curve as a function of the arclength s. The rationale behind this change is that the new speed is always one, i.e., $\|\dot{\boldsymbol{v}}(s)\| = 1$. In what follows, derivation with respect to arclength s will be denoted by an overdot.

If the chain rule is applied to the first-time derivative of the curve, we obtain

$$\begin{aligned} \boldsymbol{v}' &= \frac{d\boldsymbol{v}}{dt} = \frac{d\boldsymbol{v}}{ds}\frac{ds}{dt} = \dot{\boldsymbol{v}}s' \\ \dot{\boldsymbol{v}} &= \frac{\boldsymbol{v}'}{s'} = \frac{\boldsymbol{v}'}{\|\boldsymbol{v}'\|} = \boldsymbol{u} \end{aligned} \tag{12}$$

with $s' = v' = \|\boldsymbol{v}'\|$ by virtue of (9). Higher order derivates can be computed but with a much more intricate algebraic structure than (12) as shown in [25].

It is interesting to note that vector $\boldsymbol{u}$ is unitary by definition and tangent to the curve by construction (see Fig. 3). Certainly, this vector can change direction but not magnitude along the curve. This fact has an immediate consequence, namely, it is possible to find another special vector that is always orthogonal to $\boldsymbol{u}$. Multiplying the second expression in (12) by $\boldsymbol{u}$ and taking the derivative of the result, we get

$$\frac{d(\boldsymbol{u}\boldsymbol{u})}{dt} = \boldsymbol{u}'\boldsymbol{u} + \boldsymbol{u}\boldsymbol{u}' = 2\boldsymbol{u}' \cdot \boldsymbol{u} = 0 \tag{13}$$

where the property $\boldsymbol{u}' \cdot \boldsymbol{u} = \frac{1}{2}(\boldsymbol{u}'\boldsymbol{u} + \boldsymbol{u}\boldsymbol{u}')$ has been used. As a consequence, the tangent vector and its first derivative are always orthogonal

$$\boldsymbol{u} \cdot \boldsymbol{u}' = \boldsymbol{u} \cdot \dot{\boldsymbol{u}} = 0 \tag{14}$$

This is equivalent to say that a simple bivector $\boldsymbol{\Omega}_1$ exists [26], such that

$$\boldsymbol{u}' = \boldsymbol{u} \cdot \boldsymbol{\Omega}_1 \tag{15}$$

with

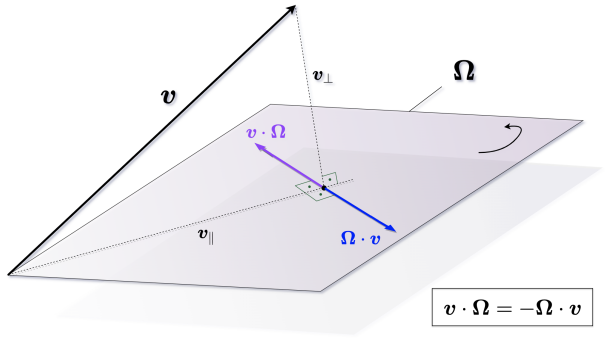

Figure 4. The dot product of a generic vector $\boldsymbol{v}$ and a simple bivector $\boldsymbol{\Omega}$. The result is a vector that lies in the plane defined by $\boldsymbol{\Omega}$ and is orthogonal to $\boldsymbol{v}_{\parallel}$ (the projection of $\boldsymbol{v}$ onto $\boldsymbol{\Omega}$). Left and right multiplication give opposite results.

$$\boldsymbol{\Omega}_1 = \boldsymbol{u}\boldsymbol{u}' = \boldsymbol{u} \wedge \boldsymbol{u}' = \frac{\boldsymbol{v}' \wedge \boldsymbol{v}''}{v'^2} = (\boldsymbol{v}')^{-1} \wedge \boldsymbol{v}'' \tag{16}$$

The simple bivector $\boldsymbol{\Omega}_1$ will be revealed as a pivotal element later on. Expression (15) has a clear interpretation. It is possible to obtain the time derivative of the unit tangent vector $\boldsymbol{u}$ by performing the dot product of this vector and a special bivector $\boldsymbol{\Omega}_1$. Geometrically, equation (15) represents the orthogonal projection onto the plane defined by the bivector $\boldsymbol{\Omega}_1$ followed by a rotation of 90º in that plane (see Fig. 4). Note that, in this particular case, $\boldsymbol{u}$ is already contained in the plane represented by the bivector $\boldsymbol{\Omega}_1$. Note also that expressions (15) and (16) are valid for arbitrary dimensions.

2) Local Orthogonal Frames and Scaled Curvatures: Attached to the curve $\boldsymbol{v}$, a moving orthogonal frame $\{\boldsymbol{u}_1, \boldsymbol{u}_1, \ldots, \boldsymbol{u}_m\}$ with $m \leq n$ and its corresponding orthonormal frame $\{\boldsymbol{e}_1, \boldsymbol{e}_1, \ldots, \boldsymbol{e}_m\}$ that travels with the curve are defined. It is known as the generalized Frénet-Serret frame or FS for short.

By choosing $\boldsymbol{e}_1 = \boldsymbol{u}$, the FS is called *mobile* or *comoving frame*. The remaining basis vectors are readily obtained by application of an orthogonalization method (such as the Gram-Schmidt process) to the n derivatives of $\boldsymbol{v}$ with respect to arc-length, i.e., $\{\dot{\boldsymbol{v}}, \ddot{\boldsymbol{v}}, \ldots, \partial_s^n \boldsymbol{v}\}$ provided that they are linearly independent. However, this is not always the case, resulting in $m \leq n$ elements. It is interesting to recall the relationship between the FS vectors and their first arc-length derivative. Assuming $m = n$, it can be expressed through the following generalized Frénet-Serret equations

$$\begin{aligned}
\dot{\boldsymbol{e}}_1 &= \kappa_1 \boldsymbol{e}_2 \\
\dot{\boldsymbol{e}}_2 &= -\kappa_1 \boldsymbol{e}_1 + \kappa_2 \boldsymbol{e}_3 \\
\dot{\boldsymbol{e}}_3 &= -\kappa_2 \boldsymbol{e}_2 + \kappa_3 \boldsymbol{e}_4 \\
&\ldots \\
\dot{\boldsymbol{e}}_n &= -\kappa_{n-1} \boldsymbol{e}_{n-1}
\end{aligned} \tag{17}$$

where the so-called curvatures κ_i can be obtained as [27]

$$\kappa_i = \dot{\boldsymbol{e}}_i \cdot \boldsymbol{e}_{i+1} = \frac{\|\boldsymbol{u}_{i+1}\|}{\|\boldsymbol{u}_i\|} \tag{18}$$

According to the chain rule presented in (12), the first time- and arc-length derivatives are related by $\boldsymbol{e}_i' = v' \dot{\boldsymbol{e}}_i$, which leads to the following time-dependant Frénet-Serret equations

$$\begin{aligned}
\boldsymbol{e}_1' &= k_1 \boldsymbol{e}_2 \\
\boldsymbol{e}_2' &= -k_1 \boldsymbol{e}_1 + k_2 \boldsymbol{e}_3 \\
\boldsymbol{e}_3' &= -k_2 \boldsymbol{e}_2 + k_3 \boldsymbol{e}_4 \\
&\ldots \\
\boldsymbol{e}_n' &= -k_{n-1} \boldsymbol{e}_{n-1}
\end{aligned} \tag{19}$$

where the values k_i are known as *scaled* curvatures,

$$k_i = v' \kappa_i = \boldsymbol{e}_i' \cdot \boldsymbol{e}_{i+1} \tag{20}$$

Scaled curvatures k_i are preferred over conventional curvatures κ_i for application in electrical engineering since electrical curves are ultimately dependent on the time parameter t.

3) Darboux Blades: One of the main contributions of this work is the introduction of the Darboux blades in the context of electrical engineering. They are 2D objects in a high-dimensional Euclidean space that represent planes of rotation. Using the generalized FS frame and scaled curvatures k_i, the simple bivector in (16) can be generalized into a set of $m-1$ simple bivectors

$$\begin{aligned}
\boldsymbol{\Omega}_1 &= k_1 \boldsymbol{e}_1 \wedge \boldsymbol{e}_2 = k_1 \boldsymbol{e}_{1,2} \\
\boldsymbol{\Omega}_2 &= k_2 \boldsymbol{e}_2 \wedge \boldsymbol{e}_3 = k_2 \boldsymbol{e}_{2,3} \\
&\vdots \\
\boldsymbol{\Omega}_{m-1} &= k_{m-1} \boldsymbol{e}_{m-1} \wedge \boldsymbol{e}_m = k_{m-1} \boldsymbol{e}_{m-1,m}
\end{aligned} \tag{21}$$

Clearly, the norm for every Darboux simple bivector is $\|\boldsymbol{\Omega}_i\| = k_i$. By virtue of (19) and (21), the following can be proved

$$\boldsymbol{e}_i' = \boldsymbol{e}_i \cdot \boldsymbol{\Omega} \tag{22}$$

Similar to the discussion in chapter 6 of [7], $\boldsymbol{\Omega}_i$ can by made into a single bivector by simple summation

$$\begin{aligned}
\boldsymbol{\Omega} &= \sum_{i=1}^{m} \boldsymbol{\Omega}_i = \sum_{i=1}^{m-1} k_i \boldsymbol{e}_{i,i+1} = \frac{1}{2} \sum_{i=1}^{m} \boldsymbol{e}_i \wedge \boldsymbol{e}_i' \\
&= v' \sum_{i=1}^{m-1} \boldsymbol{u}_i^{-1} \wedge \boldsymbol{u}_{i+1}
\end{aligned} \tag{23}$$

with norm given by

$$\|\boldsymbol{\Omega}\| = \sqrt{\langle \boldsymbol{\Omega}^\dagger \boldsymbol{\Omega} \rangle_0} = \sqrt{\sum_{i=1}^{m-1} k_i^2} \tag{24}$$

For the special case of a 3-dimensional space, it reduces to $\|\boldsymbol{\Omega}\| = \sqrt{k_1^2 + k_2^2}$. Expressions in Eq. (21) account for orthogonal angular velocity bivectors of the moving FS frame, i.e., each $\boldsymbol{\Omega}_i$ represents an instantaneous plane of rotation in n dimensions. The bivector $\boldsymbol{\Omega}$ is called the *Darboux Bivector* (DB) because it directly generalizes the classical Darboux vector to higher dimensions. Moreover, the set of Darboux simple bivectors, and by extension their sum (23), summarizes the geometrical properties of a curve in a single convenient quantity.

Note that while each $\boldsymbol{\Omega}_i$ is a simple bivector that represents a plane, the sum $\boldsymbol{\Omega}$ is generally not a simple bivector, except in 2 and 3-dimensions. The interpretation for $\boldsymbol{\Omega}$ is that it accounts for the instantaneous angular speed of the FS frame.

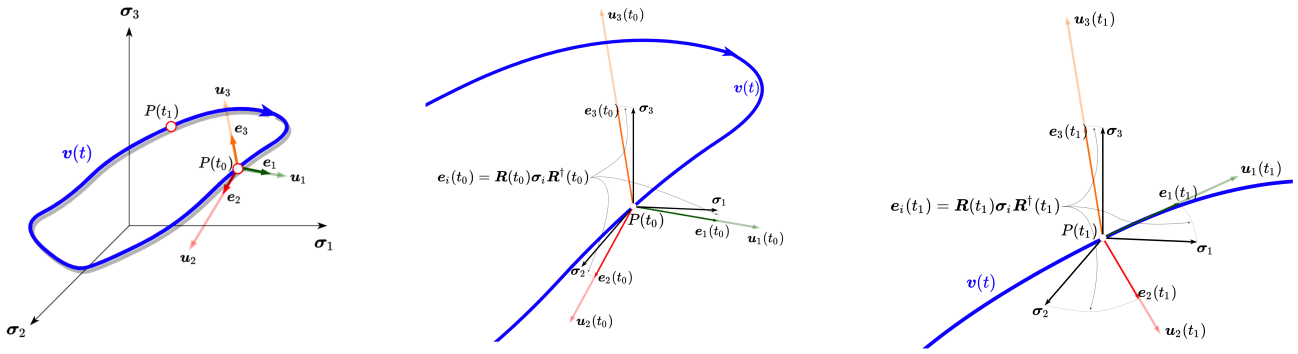

Figure 5. Frénet-Serret frame for a three-dimensional system travelling along an electrical curve (left). At instant t_0 the associated rotor $\boldsymbol{R}(t_0)$ rotates the fixed basis $\boldsymbol{\sigma}$ to FS frame $\boldsymbol{e}(t_0)$ (middle). The same curve for time t_1 and associated rotor $\boldsymbol{R}(t_1)$ (right) .

The rationale for this interpretation stems from considering the rotation of the fixed basis vectors $\boldsymbol{\sigma}_i$ to match the mobile FS basis vectors $\boldsymbol{e}_i$ (see figure 5). The rotational motion of these vectors is determined by a time-varying geometric rotor $\boldsymbol{R}(t)$, such that

$$\boldsymbol{e}_i(t) = \boldsymbol{R}(t)\boldsymbol{\sigma}_i\boldsymbol{R}^\dagger(t) \tag{25}$$

where $\boldsymbol{R}\boldsymbol{R}^\dagger = \boldsymbol{R}\boldsymbol{R}^{-1} = 1$.

By performing the derivative of equation (25) with respect to time and after some algebraic manipulations, the following expression is obtained

$$\boldsymbol{\Omega} = 2\boldsymbol{R}'\boldsymbol{R}^{-1} = -\boldsymbol{\Omega}^\dagger \tag{26}$$

Note that for 2D and 3D, both $\boldsymbol{\Omega}$ and $\boldsymbol{R}$ are always bivectors [28]. In higher dimensions, $\boldsymbol{R}$ can include higher even grade elements, however, $\boldsymbol{\Omega}$ remains as a bivector. Solving equation (26) is equivalent to solving the system of equations in (17).

Using the rotor $\boldsymbol{R}$ as a linear transformation, the spatial curve described by vector $\boldsymbol{v}$ can be converted into a general piecewise straight line $\boldsymbol{v}_{FS}$ in the mobile reference frame. This is quite similar to a DC quantity as highlighted by Milano in [29]. This new transformation should be considered equivalent to decoupling the variation in frequency from the amplitude of the vector signal involved. This geometric technique has recently been applied successfully by the authors in [30] and it deserves further exploration in future works to test a reduction of the complexity in the control loop of the system by switching from the fixed reference frame to the moving one.

III. Geometry in multi-phase power systems

In this section, we present the main ideas that relate to the geometrical aspects associated with space curves as described in the previous section with the notion of vector representation in power systems. Specifically, we are mostly interested in the interpretation of frequency. Interestingly, even though we all have a more or less clear notion associated with the repetition of something in time, nowadays the scientific community still does not agree when it comes to instantaneous frequency (IF), that is to say, there is no clear agreement to define what the frequency means for a specific instant of time [14], [31]. From the authors' point of view, perhaps the geometric association proposed in this paper can shed light on the problem. The concept of angular velocity, which is widely used in mechanical systems, does have an immediate physical translation: it is a measurement of rotation rate referring to how fast an object rotates, i.e. how fast the angular position or orientation of an object changes with time. This is the case of the moving FS frame previously presented. It rotates in space according to the DB, encoding the plane/s of rotation and angular speed. The importance of this bivector is highlighted in the remainder of the text. We also emphasize discussing a comprehensive concept of frequency, not limited to a specific electrical single-phase, but linked to the multi-phase system as a whole. Additionally, the concept of Rate of Change of Frequency (RoCoF) is also linked to the derivative of DB as a measure of the available inertia in the system [31].

A. Geometric voltage in multi-phase circuits and angular frequency as intrinsic property

Let's consider the voltages (or currents) of a multi-phase power system with a number of phases $n \geq 2$ (see next section for the special case $n = 1$). They can be arranged to form a vector describing a curve in space, known as *electrical curve* (EC). For simplicity, we will focus on voltage, although the same can be applied to the current. The geometric voltage is defined as in equation (3), where the coordinates v_i can be line-to-line (LL), line-to-neutral (LN) or line-to-virtual neutral (LVN) voltages,

$$\boldsymbol{v} = v_1\boldsymbol{\sigma}_1 + v_2\boldsymbol{\sigma}_2 + \ldots + v_n\boldsymbol{\sigma}_n \tag{27}$$

Note that n can be the number of phases or wires, depending on the specific application. By analysing the intrinsic properties of the curve $\boldsymbol{v}$, i.e., the scaled curvatures k_i and the Darboux Bivector $\boldsymbol{\Omega}$, a general concept of frequency can be established. One of the main results of this work is to propose that the angular frequency of the multi-phase system as a whole is encoded in the above-mentioned intrinsic properties k_i and $\boldsymbol{\Omega}$. The coordinates of DB also provide information about the rotation in specific planes. Fig. 6 shows a diagram with the main parts of this process.

B. Special cases: DC and single-phase circuits

The study of single-phase or DC systems through differential geometry presents a severe drawback for natural reasons: in one dimension there are no associated curvatures, and therefore, there is no way to compute the DB. By virtue of (3), the geometric voltage is

$$\boldsymbol{v} = v\boldsymbol{\sigma}_1 \tag{28}$$

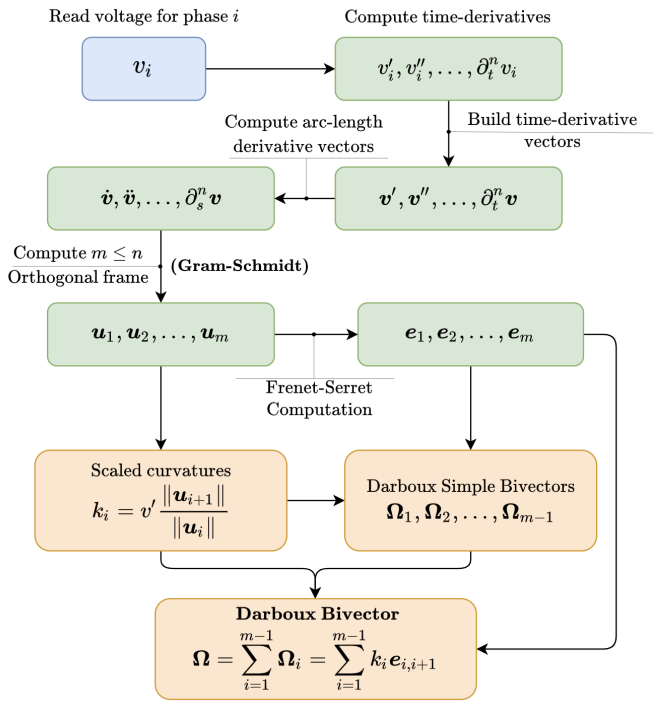

Figure 6. Flowchart of the proposed method for computation of the Darboux Bivector and scaled curvatures.

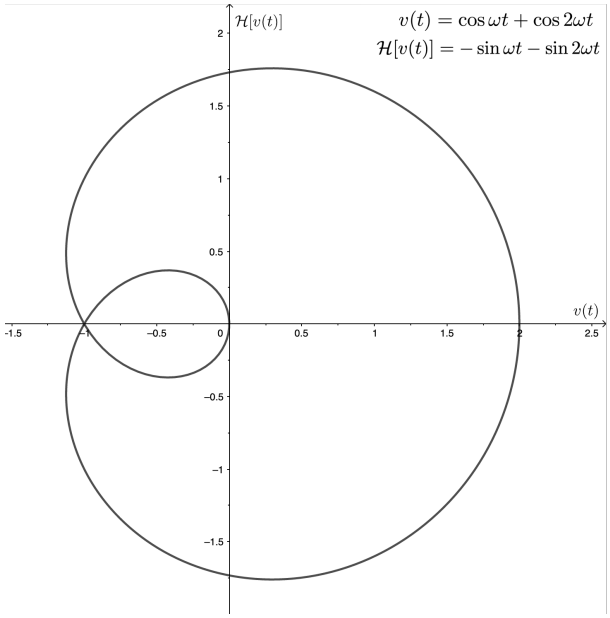

Figure 7. Complex representation of a harmonic voltage using the Hilbert Transform. The curvature κ is not constant for a constant frequency signal.

A one-dimensional manifold does not have any intrinsic curvature at all. It is always locally isometric to a straight, "flat" line. Intrinsic curvature only makes sense in 2 or more dimensions. Thus, unless additional assumptions are made, IF computation is not feasible in single-phase or DC power systems. To overcome this issue in AC systems, an additional dimension is commonly added through the use of quadrature methods and complex algebra. For example, in [18] the Hilbert transform (HT) is employed to create an analytic signal. However, this only works well for purely sinusoidal systems, but not for non-sinusoidal ones [32]. As an example, consider the harmonic voltage $v(t) = \cos\omega t + \cos 2\omega t$ with constant angular frequency ω. Fig. 7 shows the curve associated with the complex analytic signal $\bar{v}(t) = v(t) + j\mathcal{H}[v(t)]$, where $\mathcal{H}$ is the HT operator. By simple inspection, it is evident that the associated curvature is not constant, in contrast to the frequency of the system. This appears to be a disputable flaw in [18]. The problem is that it is not possible to find the right IF value of a signal without prior information about its structure [33], so IF becomes meaningless. A possible solution for this issue is to use hypercomplex representation as presented in [34].

IV. Analytical Formulation for Sinusoidal Supply

In this section, the main analytical derivations for n-phase systems are presented for sinusoidal AC systems. Due to their significance, three-phase systems are included as a particular case. The software Mathematica and WolframAlpha have been used for symbolic computation, along with the GeometricAlgebra FulcrumLib library [35] which has greatly simplified the calculations. For more elaborated voltages, including harmonics or transients, the analytical solution becomes more intricate and tedious, so it adds no value to disclose it here. Numerical results for realistic cases will be presented in section V.

A. Three-phase AC system

This section presents the case of a three-phase AC system. It can be 4- or 3-wire depending on the presence of a neutral conductor or not. This circumstance enables the definition of either a set of 4 LL voltages (more specifically, wire-to-wire) or 3 line-to-common-wire voltages (referred to the same conductor, usually the neutral wire or n). In the most general case, the voltages referred to the neutral wire need not add up to zero, i.e. $v_{an} + v_{bn} + v_{cn} \neq 0$. In contrast, line voltages always add up to zero because of KVL, i.e., $v_{ab} + v_{bc} + v_{cn} + v_{na} = 0$. Some authors make use of the so-called virtual neutral N to form another set of zero-sum voltages $v_{aN} + v_{bN} + v_{cN} + v_{nN} = 0$. Regardless of the chosen strategy, it will be shown that the results remain similar at the geometrical level since the resulting curve is confined to a three-dimensional space. For the particular case of 3 wires, it will be shown in section IV-C that a reduction of one dimension can be carried out because of KVL.

Here, sinusoidal AC systems with symmetrical and non-symmetrical voltages will be analyzed. We select the phase-to-neutral voltages

$$\begin{aligned} v_a(t) &= \sqrt{2} V_a \cos(\omega t) \\ v_b(t) &= \sqrt{2} V_b \cos(\omega t + \varphi_b) \\ v_c(t) &= \sqrt{2} V_c \cos(\omega t + \varphi_c) \end{aligned} \tag{29}$$

where $\varphi_a = 0$ for simplicity. According to (3), the voltage vector is

$$\boldsymbol{v} = v_a \boldsymbol{\sigma}_1 + v_b \boldsymbol{\sigma}_2 + v_c \boldsymbol{\sigma}_3$$

1) Symmetrical voltage: For the symmetric and positive sequence case, i.e., $V_a = V_b = V_c = V$ and $\varphi_b = -\varphi_c = -\frac{2\pi}{3}$, the resulting curve is the well-known circle in 3D space. Of course, the angular frequency ω is constant. For this particular case, it suffices the application of Eq. (16), resulting in the following simple DB

$$\boldsymbol{\Omega} = \frac{\omega}{\sqrt{3}} \left(\boldsymbol{\sigma}_{12} + \boldsymbol{\sigma}_{23} + \boldsymbol{\sigma}_{31}\right)$$

with $\|\boldsymbol{\Omega}\| = \omega$. As explained in previous sections, $\boldsymbol{\Omega}$ encodes the plane of rotation of the FS along the curve, while $\|\boldsymbol{\Omega}\|$ is the angular velocity, which coincides with the electrical angular frequency for this particular case. The application of Gram-Schmidt procedure and equation (22) provide the unit vectors $\boldsymbol{e}_1$ and $\boldsymbol{e}_2$ that span the plane of rotation

$$\begin{aligned}
\boldsymbol{e}_1 &= -\sqrt{\frac{2}{3}} \left[\sin(\omega t)\boldsymbol{\sigma}_1 + \sin\left(\omega t - \tfrac{2\pi}{3}\right)\boldsymbol{\sigma}_2 + \sin\left(\omega t + \tfrac{2\pi}{3}\right)\boldsymbol{\sigma}_3\right] \\
\boldsymbol{e}_2 &= -\sqrt{\frac{2}{3}} \left[\cos(\omega t)\boldsymbol{\sigma}_1 + \cos\left(\omega t - \tfrac{2\pi}{3}\right)\boldsymbol{\sigma}_2 + \cos\left(\omega t + \tfrac{2\pi}{3}\right)\boldsymbol{\sigma}_3\right] \\
\boldsymbol{e}_1' &= \omega \boldsymbol{e}_2 \\
\boldsymbol{e}_2' &= -\omega \boldsymbol{e}_1
\end{aligned}$$

Note also that the DB can be expressed in the FS frame as $\boldsymbol{\Omega} = k_1 \boldsymbol{e}_{12} = \omega \boldsymbol{e}_{12}$ as stated in equation (23), i.e., it rotates (but not twist) clockwise in the plane of the circle.

The case of negative sequence is straightforward. Changing roles for v_{bc} and v_{ca} in (29), the new DB results in $\boldsymbol{\Omega}_- = -\boldsymbol{\Omega}$. It is the same curve with the same angular velocity and the same frequency but rotating counterclockwise, i.e., $\boldsymbol{\Omega} = \omega \boldsymbol{e}_{21}$. Note that for a zero sequence system, $\boldsymbol{\Omega} = 0$, i.e., a straight line is obtained for the voltage curve. Therefore, we are in the same case as in section III-B.

2) Asymmetrical voltage: For this case, we limit ourselves to the case of $V_a \neq V_b \neq V_c$ and $\varphi_b = -\varphi_c = -\frac{2\pi}{3}$, for simplicity. Realistic general cases will be considered in the next section. As in the symmetrical case, the electrical curve also lies in a plane, so the application of (16) now gives

$$\boldsymbol{\Omega} = \frac{\sqrt{3}\omega^3}{v'^2} \left(V_a V_b \boldsymbol{\sigma}_{12} + V_b V_c \boldsymbol{\sigma}_{23} + V_c V_a \boldsymbol{\sigma}_{31}\right)$$

$$\|\boldsymbol{\Omega}\| = \Omega = \frac{\sqrt{3}\omega^3 V}{v'^2}$$

with

$$\begin{aligned}
v'^2 &= 2\omega^2 \left(V_a^2 \sin^2(\omega t) + V_b^2 \sin^2\left(\omega t - \tfrac{2\pi}{3}\right) + V_c^2 \sin^2\left(\omega t + \tfrac{2\pi}{3}\right)\right) \\
V &= \sqrt{V_a^2 V_b^2 + V_b^2 V_c^2 + V_c^2 V_a^2}
\end{aligned}$$

In this case, the angular velocity is not constant and depends not only on the electrical angular frequency ω but also on the amplitude of the voltages V_a, V_b and V_c. It is interesting to note that the plane of rotation is different from that of the balanced case. It changes according to the values of the amplitudes of the voltages. This fact provides invaluable information for the study of the asymmetry of the system and deserves further investigation. The scaled curvature is readily obtained as

$$k_1 = \Omega = \Omega_1 = \frac{\sqrt{3}\omega^3 V}{v'^2}$$

If we now compute the derivative of $\boldsymbol{\Omega}$, the geometric counterpart of RoCoF is obtained

$$\boldsymbol{\Omega}' = \frac{d\boldsymbol{\Omega}}{dt} = -\frac{2v''}{v'}\boldsymbol{\Omega} \tag{30}$$

Note that v'' is null for symmetrical voltages, so is $\boldsymbol{\Omega}'$ as expected.

B. General sinusoidal n-phase AC systems

The sequence described in Fig. 6 is completely general and can be applied to any kind of voltage supply with any number of phases. This section presents the analytical solution for the typical case of use concerning highly sinusoidal networks (low level of harmonic) but with potential asymmetries. In the Example section, the method is applied for arbitrary harmonic voltages, including transients and distortions.

For an n-phase system, the geometrical voltage describes an electrical curve given by

$$\begin{aligned}
\boldsymbol{v} &= \sum_{i=1}^{n} \sqrt{2} V_i \cos\left(\omega t - \varphi_i\right) \boldsymbol{\sigma}_i \\
&= \sum_{i=1}^{n} \sqrt{2} \left(V_i \cos\varphi_i \cos\omega t + V_i \sin\varphi_i \sin\omega t\right) \boldsymbol{\sigma}_i \\
&= \cos\omega t \left[\sum_{i=1}^{n} \sqrt{2} V_i \cos\varphi_i \boldsymbol{\sigma}_i\right] + \sin\omega t \left[\sum_{i=1}^{n} \sqrt{2} V_i \sin\varphi_i \boldsymbol{\sigma}_i\right] \\
&= \cos\omega t\, \boldsymbol{a} + \sin\omega t\, \boldsymbol{b}
\end{aligned}$$

with

$$\boldsymbol{a} = \sum_{i=1}^{n} \sqrt{2} V_i \cos\varphi_i \boldsymbol{\sigma}_i \quad \boldsymbol{b} = \sum_{i=1}^{n} \sqrt{2} V_i \sin\varphi_i \boldsymbol{\sigma}_i$$

Thus, the vector $\boldsymbol{v}$ describes an elliptical curve in the plane determined by the n-dimensional vectors $\boldsymbol{a}$ and $\boldsymbol{b}$. The first two derivatives of this signal are:

$$\begin{aligned}
\boldsymbol{v}' &= \omega \left(-\sin\omega t\, \boldsymbol{a} + \cos\omega t\, \boldsymbol{b}\right) \\
\boldsymbol{v}'' &= -\omega^2 \left(\cos\omega t\, \boldsymbol{a} + \sin\omega t\, \boldsymbol{b}\right) = -\omega^2 \boldsymbol{v}
\end{aligned}$$

They are linear combinations of vectors $\boldsymbol{a}$ and $\boldsymbol{b}$, so they are in the same plane as the vector $\boldsymbol{v}$. The general expressions for all even and odd-time derivatives are

$$\begin{aligned}
\boldsymbol{v}^{(2m)} &= (-1)^m \omega^{2m} \boldsymbol{v} \\
\boldsymbol{v}^{(2m+1)} &= (-1)^m \omega^{2m} \boldsymbol{v}' \\
m &\in \{1, 2, \ldots\}
\end{aligned}$$

This means that all higher derivatives $\boldsymbol{v}^{(k)}$ with $k > 1$ are linearly dependent on $\boldsymbol{v}$ or $\boldsymbol{v}'$, hence belong to the plane defined by $\boldsymbol{a}$ and $\boldsymbol{b}$. In GA, this plane can be represented by the 2-blade $\boldsymbol{K} = \boldsymbol{a} \wedge \boldsymbol{b}$ (see Fig. 1). Using the above results, the DB can be computed as in equation (16)

$$\boldsymbol{\Omega} = \frac{\boldsymbol{v}' \wedge \boldsymbol{v}''}{v'^2} = \frac{\omega^3}{v'^2} \boldsymbol{K} \tag{31}$$

Because $\boldsymbol{K}$ does not depend on time, the expression for RoCoF is the same as in (30). It is evident that both, $\boldsymbol{\Omega}$ and $\boldsymbol{\Omega}'$ are scaled versions of the 2-blade $\boldsymbol{K}$ with time-dependent scale factors.

C. General Rotations and Frénet-Serret frame

Matrix-based linear maps like Clarke or Park transformations are widely used in electrical systems. They can be considered

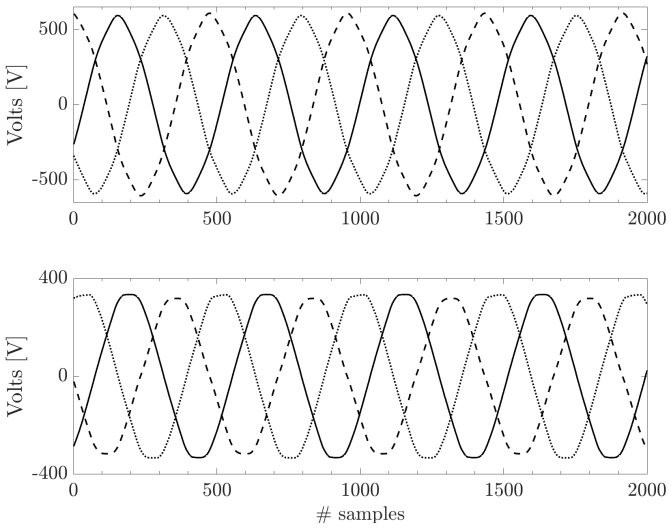

Figure 8. Three-phase LL (top) and LN (bottom) voltages for a real building in example A). The signals are polluted mainly with 3rd, 5th and 7th harmonics.

as general rotations in the Euclidean space [4], [36]. In GA, rotations are accomplished employing geometric rotors [30].

Based on the geometrical interpretation of voltage or current signals adopted in this work, multi-phase AC voltages can be studied from a simplified conceptual and dimensional point of view by applying an adequate rotation to the basis $\boldsymbol{\sigma}$ defined in (1). The result is that vector $\boldsymbol{v}$ is now represented as $\boldsymbol{v}_T$ in a new basis using a reduced number of coordinates and/or leading to a simplified shape. For example, for a three-phase system, Park transform allows describing vector $\boldsymbol{v}$ exclusively by a linear combination of only two basis vectors (say $\boldsymbol{d}$ and $\boldsymbol{q}$) lying in the plane represented by bivector $\boldsymbol{K}$ and rotating at an arbitrary speed ω_P. Additionally, as shown in Section II-B3, it is also possible to find a new transformation based on the rotation of the FS frame that transforms the electrical curve into a simplified piecewise straight line. Interestingly enough, this fact holds for any sinusoidal multi-phase system with a number of phases greater than 2, as outlined in the previous sections.

V. Examples

Several simulations and real-world examples are presented and analyzed hereafter to validate the proposed framework in this paper. First, a steady-state harmonic voltage measured in an educational building at the University of Almeria (Spain) is presented. Secondly, the simulation of a transient due to a fault in the IEEE34 network is reported.

A. Three phase AC voltage with harmonics

In this section, harmonic polluted signals obtained in the low voltage panel of an academic building at the University of Almeria (Spain) are analyzed. Fig. 8 shows the LL (top) and LN (bottom) voltages acquired using the openzmeter device [37] at a sampling frequency of 24 kHz. The nominal frequency of the grid is 50 Hz. Some waveform distortion caused by the harmonic content (mainly third, fifth and seventh harmonics) is noticeable. Fig. 9 shows the electrical curve for the LN voltage from different viewing angles. It can be seen that the curve is not exactly a circle but a hexagon because of the harmonic

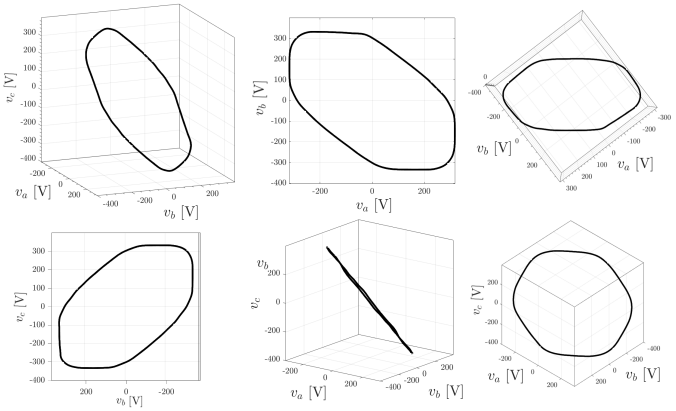

Figure 9. Electrical curve for LN voltages in a real building in example A). Different views are presented. Note that the curve does not exactly lie in a plane as shown in the lower-centred subfigure.

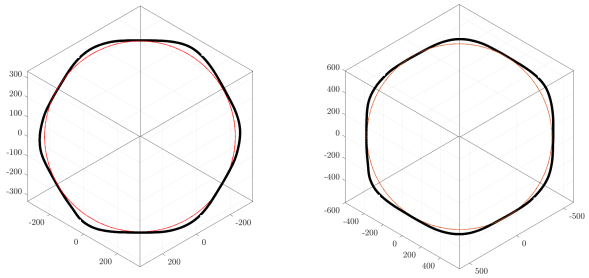

Figure 10. Orthogonal view for electrical curves for LN (left) and LL (right) voltages. The red circles represent nominal voltage with radius $r_{LN} = 230\sqrt{3}$ (LN) and $r_{LL} = 400\sqrt{3}$ (LL).

content. Moreover, it does not lie in a plane either since there is a zero sequence component, i.e., $v_a + v_b + v_c \neq 0$. Fig. 10 shows a comparison of the shape for the LL and LN electrical curves. The non-circularity of both curves is indeed observed. Note that, unlike the curve for the LN voltages, the LL curve is contained in a plane.

The computation of DB is based on the integral of expression (23) for better numerical stability. The result is shown in Fig. 11. It is interesting to note that due to harmonics, the instantaneous angular frequency is not constant although its mean value (313.98 rad/s) is very close to the nominal angular frequency of the grid ($\omega_{\text{nom}} = 314.15$ rad/s). Note also that $\|\boldsymbol{\Omega}\|$ is a periodic curve, with a period of exactly 240 samples, i.e., 50 Hz. The above results were obtained using a simple kernel average smoothing linear interpolation method [38] which allows for

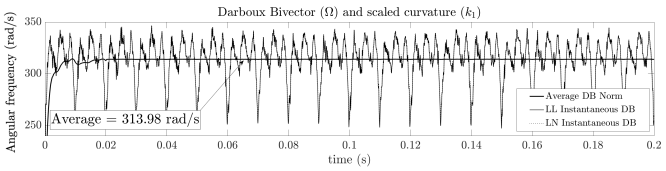

Figure 11. Instantaneous angular frequency DB $\|\boldsymbol{\Omega}\|$ for LN and LL voltages. The mean value of the DB is 313.98 rad/s for both LL and LN which is very close to the nominal angular frequency grid ($\omega = 314.15$ rad/s).

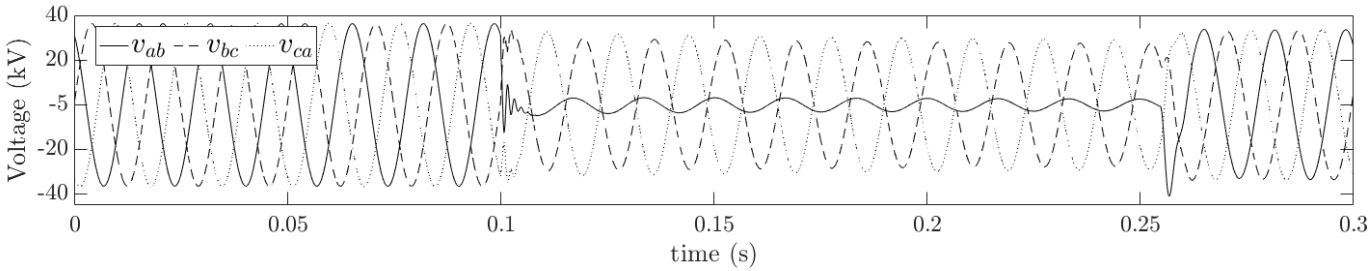

Figure 12. Three-phase line voltages at bus 832 at the IEEE 34-bus system. A line-to-line fault in bus 854 starts at $t = 0.1$s. The fault is cleared at $t = 0.25$s.

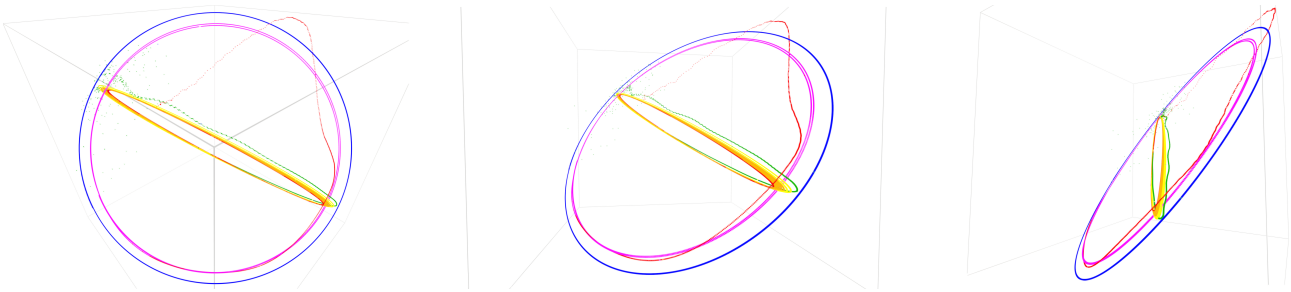

Figure 13. Different views of the point-cloud-like electrical curve for the LN voltage. The colours encode different stages in the transient evolution

obtaining accurate first and second derivatives.
It should be emphasized that it is recommended to use the line-to-line voltage as the preferred electrical curve due to its differential nature, which ensures greater numerical stability and reduced noise. Furthermore, this approach allows for a one-dimensional reduction of the problem compared to the phase-to-neutral voltage curve.

B. Fault in IEEE34-bus network

This second example shows the application of the proposed method to estimate the DB at a bus of a power system under faulty conditions. To this aim, the IEEE 34-bus model provided by EMTP is used to perform a transient simulation. A line-to-line fault has been generated between phases a and b at terminal bus 854 of the system at $t = 0.1$s. The fault is cleared at $t = 0.25$s. The integration time step considered is 10^{-6}s. The line voltages at bus 832 during pre- and post-fault are shown in Fig. 12. A point-cloud-like electrical curve is depicted in Fig. 13 for the LN voltages. Different colours are assigned to highlight different stages in the waveforms. The outermost circle (blue) represents the initial steady state condition. At around $t = 0.1$s, a fault produces a transient (dark green) that evolves in a new distorted steady state represented by several ellipses (green, yellow and orange). At around $t = 0.25$s, the fault starts to clear (purple) and finally, a new steady state is reached (red) depicted by the inner circle (with a lower voltage magnitude). Note that all the points are nearly contained in a plane, except for the transient part (dark green) that is scattered around the vicinity of the plane in 3D space.

Figure 14 shows the DB for the LL voltages in the considered timespan. All the computations for the derivatives of the voltage vector have been performed by using the same linear interpolation technique as before. Initially, the three phases remain balanced and thus, the DB remains constant at an angular frequency close to the nominal value of the grid, i.e., 377 rad/s (60 Hz). The same holds after the fault

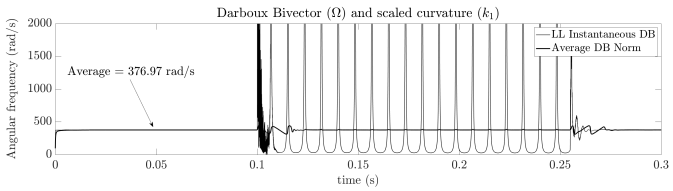

Figure 14. Instantaneous angular frequency DB $\|\boldsymbol{\Omega}\|$ for LL voltages. The mean value of the DB before the transient is 376.97 rad/s which is very close to the nominal angular frequency grid ($\omega = 376.99$ rad/s).

clearance. Interestingly enough, the DB suffers heavy but periodic oscillations during the fault that are consistent with an elliptical motion (as shown in Fig. 13). The mean value of this oscillation matches again the nominal angular frequency of the grid. In the same vein as in the previous example, the electrical line-to-line curve lies in a plane and thus, only the scaled curvature k_1 is non-null.

VI. Conclusions

In this paper, we have presented a novel approach for the analysis of multi-phase power systems using geometric algebra and differential geometry. We have extended the concept of geometric frequency to arbitrary n-phase systems by introducing the *Darboux Bivector* and *Electrical Curves*, which characterize voltage or current in multi-phase AC systems. This breakthrough allows for a more comprehensive understanding of frequency in multi-phase power systems and has potential applications in multi-phase electrical machines and power converters.

Our main contributions include the generalization of frequency for arbitrary multi-phase systems, the introduction of the Darboux bivector for electrical curves, the introduction of scaled curvatures, and the determination of restrictions for the validity of the method in single-phase and DC circuits. We have also demonstrated how the geometric algebra framework unifies

mathematical concepts and provides a clearer understanding of these systems, which can benefit educational settings.

This work not only sheds new light on the study of multi-phase power systems but also highlights the benefits of using geometric algebra and differential geometry in the engineering field.

VII. Future Work

Future work may involve exploring the application of our findings to specific multi-phase power systems or investigating the potential benefits of this approach in other areas of electrical engineering. Additionally, the development of new visualization techniques using geometric algebra can further improve the understanding and analysis of these complex systems.

As anticipated by Milano et al. [18], despite the increased complexity introduced by the new theoretical framework, it is worth exploring the benefits that a unified geometric perspective can bring to the study of electrical systems. For instance, the analysis of properties such as bending energy, eccentricity, or other concepts associated with characterizing curves from a geometric viewpoint may provide valuable insights for understanding power quality events or even detecting anomalies and system malfunctions.

By delving into the geometric characteristics of power systems, researchers can potentially uncover previously unexplored relationships and patterns that can improve system performance and stability. Furthermore, this geometric approach can also facilitate the development of new methods for monitoring, diagnosing, and controlling power systems, based on the inherent properties of the underlying geometric structures.

In addition to these potential benefits, the unified geometric perspective can also contribute to a more intuitive understanding of power systems, making it easier for engineers and researchers to visualize and comprehend their behaviour. This can lead to more efficient problem-solving strategies and facilitate the exchange of ideas between experts from various disciplines, ultimately resulting in a more holistic understanding of the power systems in question.

References

[1] F. Milano and Á. O. Manjavacas, *Frequency Variations in Power Systems: Modeling, State Estimation, and Control*. John Wiley & Sons, 2020.

[2] J. M. Aller, A. Bueno, and T. Pagá, "Power system analysis using space-vector transformation," *IEEE Transactions on power systems*, vol. 17, no. 4, pp. 957–965, 2002.

[3] V. do Prado Brasil, A. de Leles Ferreira Filho, and J. Y. Ishihara, "Electrical three phase circuit analysis using quaternions," in *2018 18th International Conference on Harmonics and Quality of Power (ICHQP)*. IEEE, 2018, pp. 1–6.

[4] C. J. O'Rourke, M. M. Qasim, M. R. Overlin, and J. L. Kirtley, "A geometric interpretation of reference frames and transformations: dq0, clarke, and park," *IEEE Transactions on Energy Conversion*, vol. 34, no. 4, pp. 2070–2083, 2019.

[5] A. Ustariz, E. Cano, and H. Tacca, "Tensor analysis of the instantaneous power in electrical networks," *Electric Power Systems Research*, vol. 80, no. 7, pp. 788–798, 2010.

[6] T. Needham, *Visual Differential Geometry and Forms: A Mathematical Drama in Five Acts*. Princeton University Press, 2021.

[7] D. Hestenes and G. Sobczyk, *Clifford algebra to geometric calculus: a unified language for mathematics and physics*. Springer Science & Business Media, 2012, vol. 5.

[8] A. Macdonald, *Linear and geometric algebra*. Alan Macdonald, 2010.

[9] F. G. Montoya, A. Alcayde, F. M. Arrabal-Campos, and R. Banos, "How to overcome the limitations of pq theory: Geometric algebra power theory to the rescue," in *2020 IEEE PES Innovative Smart Grid Technologies Europe (ISGT-Europe)*. IEEE, 2020, pp. 339–343.

[10] F. G. Montoya, R. Baños, A. Alcayde, F. M. Arrabal-Campos, and J. Roldán Pérez, "Geometric algebra framework applied to symmetrical balanced three-phase systems for sinusoidal and non-sinusoidal voltage supply," *Mathematics*, vol. 9, no. 11, p. 1259, 2021.

[11] F. G. Montoya, R. Baños, A. Alcayde, F. M. Arrabal-Campos, and J. Roldán-Pérez, "Vector geometric algebra in power systems: An updated formulation of apparent power under non-sinusoidal conditions," *Mathematics*, vol. 9, no. 11, p. 1295, 2021.

[12] F. Montoya, F. de León, F. Arrabal-Campos, and A. Alcayde, "Determination of instantaneous powers from a novel time-domain parameter identification method of non-linear single-phase circuits," *IEEE Transactions on Power Delivery*, 2021, "available on-line in IEEE Xplore".

[13] J. Snygg, *A new approach to differential geometry using Clifford's geometric algebra*. Springer Science & Business Media, 2011.

[14] H. Kirkham, W. Dickerson, and A. Phadke, "Defining power system frequency," in *2018 IEEE Power & Energy Society General Meeting (PESGM)*. IEEE, 2018, pp. 1–5.

[15] H. Karimi, M. Karimi-Ghartemani, and M. R. Iravani, "Estimation of frequency and its rate of change for applications in power systems," *IEEE Transactions on Power Delivery*, vol. 19, no. 2, pp. 472–480, 2004.

[16] I. Cotton, K. Kopsidas, and Y. Zhang, "Comparison of transient and power frequency-induced voltages on a pipeline parallel to an overhead transmission line," *IEEE transactions on power delivery*, vol. 22, no. 3, pp. 1706–1714, 2007.

[17] F. Milano, "A geometrical interpretation of frequency," *IEEE Transactions on Power Systems*, vol. 37, no. 1, pp. 816–819, 2022.

[18] F. Milano, G. Tzounas, I. Dassios, and T. Kerci, "Applications of the frenet frame to electric circuits," *IEEE Transactions on Circuits and Systems I: Regular Papers*, 2021.

[19] F. Barrero and M. J. Duran, "Recent advances in the design, modeling, and control of multiphase machines—part i," *IEEE Transactions on Industrial Electronics*, vol. 63, no. 1, pp. 449–458, 2015.

[20] L. de Lillo, L. Empringham, P. W. Wheeler, S. Khwan-On, C. Gerada, M. N. Othman, and X. Huang, "Multiphase power converter drive for fault-tolerant machine development in aerospace applications," *IEEE Transactions on Industrial Electronics*, vol. 57, no. 2, pp. 575–583, 2009.

[21] H. Grassmann, *Die lineale Ausdehnungslehre*. O. Wigand, 1844, vol. 1.

[22] M. Riesz, *Clifford numbers and spinors*. Springer Science & Business Media, 2013, vol. 54.

[23] P. Lounesto, "Clifford algebras and spinors," in *Clifford Algebras and Their Applications in Mathematical Physics*. Springer, 1986, pp. 25–37.

[24] D. Hestenes, "The genesis of geometric algebra: A personal retrospective," *Advances in Applied Clifford Algebras*, vol. 27, no. 1, pp. 351–379, 2017.

[25] A. H. Eid and F. G. Montoya, "A geometric procedure for computing differential characteristics of multi-phase electrical signals using geometric algebra," *arXiv preprint arXiv:2208.05917*, 2022.

[26] D. Hestenes, *New foundations for classical mechanics*. Springer Science & Business Media, 2012, vol. 15.

[27] H. Gluck, "Higher curvatures of curves in euclidean space," *The American Mathematical Monthly*, vol. 73, no. 7, pp. 699–704, aug 1966.

[28] D. Hestenes, "Proper particle mechanics," *Journal of Mathematical Physics*, vol. 15, no. 10, pp. 1768–1777, 1974.

[29] F. Milano, "The frenet frame as a generalization of the park transform," *IEEE Transactions on Circuits and Systems I: Regular Papers*, pp. 1–11, 2022.

[30] A. H. Eid and F. G. Montoya, "A systematic and comprehensive geometric framework for multiphase power systems analysis and computing in time domain," *IEEE Access*, vol. 10, pp. 132 725–132 741, 2022.

[31] A. J. Roscoe, A. Dyśko, B. Marshall, M. Lee, H. Kirkham, and G. Rietveld, "The case for redefinition of frequency and rocof to account for ac power system phase steps," in *2017 IEEE International Workshop on Applied Measurements for Power Systems (AMPS)*. IEEE, 2017, pp. 1–6.

[32] P. F. Pai, "Circular instantaneous frequency," *Advances in Adaptive Data Analysis*, vol. 2, no. 01, pp. 39–64, 2010.

[33] B. Boashash, "Estimating and interpreting the instantaneous frequency of a signal. i. fundamentals," *Proceedings of the IEEE*, vol. 80, no. 4, pp. 520–538, 1992.

[34] F. G. Montoya, R. Baños, A. Alcayde, F. M. Arrabal-Campos, and J. Roldán-Pérez, "Geometric algebra applied to multiphase electrical circuits in mixed time–frequency domain by means of hypercomplex hilbert transform," *Mathematics*, vol. 10, no. 9, p. 1419, 2022.

[35] A. H. Eid, "Geometric algebra fulcrum lib," Accessed on February 2022. [Online]. Available: https://github.com/ga-explorer/GeometricAlgebraFulcrumLib

[36] F. G. Montoya and A. H. Eid, "Formulating the geometric foundation of clarke, park, and fbd transformations by means of clifford's geometric algebra," *Mathematical Methods in the Applied Sciences*, 2021.

[37] E. Viciana, A. Alcayde, F. G. Montoya, R. Baños, F. M. Arrabal-Campos, and F. Manzano-Agugliaro, "An open hardware design for internet of things power quality and energy saving solutions," *Sensors*, vol. 19, no. 3, p. 627, 2019.

[38] M. R. Gupta, E. K. Garcia, and E. Chin, "Adaptive local linear regression with application to printer color management," *IEEE Transactions on Image Processing*, vol. 17, no. 6, pp. 936–945, 2008.